HHS Public Access

Author manuscript

Bone. Author manuscript; available in PMC 2024 February 16.

Published in final edited form as:

Bone. 2022 September ; 162: 116476. doi:10.1016/j.bone.2022.116476.

INDUCTION OF A NOTCH3 LEHMAN SYNDROME MUTATION IN OSTEOCYTES CAUSES OSTEOPENIA IN MALE C57BL/6J MICE

E. Canalis[*,1,2,3], **S.P. Yee**[4], **A.N. Economides**[5], **L. Schilling**[3], **J. Yu**[1,3]

[1]Department of Orthopaedic Surgery, UConn Health, Farmington, CT 06030

[2]Department of Medicine, UConn Health, Farmington, CT 06030

[3]UConn Musculoskeletal Institute, UConn Health, Farmington, CT 06030

[4]Department of Cell Biology, UConn Health, Farmington, CT 06030

[5]Regeneron Pharmaceuticals, Tarrytown, NY 10531

Abstract

Lateral Meningocele or Lehman Syndrome (LMS) is associated with *NOTCH3* mutations causing deletions of the PEST domain and a gain-of-NOTCH3 function. We demonstrated that *Notch3*^{em1Ecan} mice harboring *Notch3* mutations analogous to those found in LMS are osteopenic because of enhanced bone resorption. To determine the contribution of specific cell lineages to the phenotype, we created a conditional-by-inversion (*Notch3*^{COIN}) model termed *Notch3*^{em2Ecan} in which Cre recombination generates a *Notch3*^{INV} allele expressing a NOTCH3 mutant lacking the PEST domain. Germline *Notch3*^{COIN} inversion caused osteopenia and phenocopied the *Notch3*^{em1Ecan} mutant, validating the model. To induce the mutation in osteocytes, smooth muscle and endothelial cells, *Notch3*^{COIN} mice were bred with mice expressing Cre from the *Dmp1*, *Sm22a* and *Cdh5* promoters, respectively, creating experimental mice harboring *Notch3*^{INV} alleles in Cre-expressing cells and control littermates harboring *Notch3*^{COIN} alleles. *Notch3*^{COIN} inversion in osteocytes led to femoral and vertebral cancellous bone osteopenia, whereas *Notch3*^{COIN} inversion in mural *Sm22a* or endothelial *Cdh5*-expressing cells did not result in a skeletal phenotype. In conclusion, introduction of the LMS mutation in osteocytes but not in vascular cells causes osteopenia and phenocopies *Notch3*^{em1Ecan} global mutant mice.

[*]Address correspondence to: Ernesto Canalis, M.D., Department of Orthopaedic Surgery, UConn Health, Farmington, CT 06030-4037, Telephone: (860) 679-7978; Fax: (860) 679-1474; canalis@uchc.edu.

CONFLICT OF INTEREST

ANE is employed by Regeneron Pharmaceuticals. EC, SPY, LS and JY declare no conflicts of interest with the contents of this article.

CRediT Author Statement

Ernesto Canalis: Conceptualization, Validation, Formal Analysis, Resources, Writing – Original Draft, Writing – Review & Editing, Visualization, Supervision, Project Administration, Funding Acquisition; **Siu-Pok Yee**: Methodology, Resources, Writing – Review & Editing; **Aris N. Economides**: Methodology, Resources, Writing – Review & Editing; **Lauren Schilling**: Investigation, Writing - Review & Editing; **Jungeun Yu**: Validation, Formal Analysis, Investigation, Data Curation, Writing - Review & Editing, Visualization

Keywords

Mouse genetics; Notch pathway; Notch3; Lateral Meningocele Syndrome; Lehman Syndrome; Osteocyte; Osteopenia

1. INTRODUCTION

Notch receptors determine cell fate and function in a variety of tissues and organs including bone [1–3]. There are four Notch receptors, NOTCH 1–4, that are activated following interactions with ligands of the Jagged and Delta-like families, present in adjacent cells [1].

There is a degree of structural and functional overlap among the four Notch receptors. However, each Notch receptor has unique functions and specific patterns of cellular expression [3]. *Notch1*, *2* and *3* and low levels of *Notch 4* transcripts are detected in skeletal cells. Whereas, *Notch1* and *Notch2* transcripts are present in osteoblasts and osteoclasts, *Notch3* mRNA is detected in osteoblasts and osteocytes but not in the myeloid/osteoclast lineage [3–5]. NOTCH1 and NOTCH2 suppress osteoblast differentiation but NOTCH1 inhibits osteoclastogenesis whereas NOTCH2 enhances osteoclast differentiation [4, 6–9]. In contrast, NOTCH3 induces osteoclastogenesis by indirect mechanisms since it is not expressed in the myeloid lineage [10]. Previous work suggests that NOTCH3 acts by increasing the expression of receptor activator of nuclear factor-κB ligand (RANKL) in osteoblasts and osteocytes, and RANKL is required for osteoclastogenesis [10–13].

Lateral Meningocele Syndrome (LMS) or Lehman Syndrome (Online Mendelian Inheritance in Man 130720) is a rare genetic disorder characterized by craniofacial and skeletal abnormalities, meningoceles and neuromuscular dysfunction [14–16]. LMS is associated with short deletions or non-sense mutations in exon 33 of *NOTCH3* that cause an early termination of translation and result in a NOTCH3 protein product that lacks the proline (P), glutamic acid (E), serine (S) and threonine (T) (PEST) domain [17]. Since the PEST domain is required for the degradation of NOTCH3, it is believed that its absence results in the stabilization of the NOTCH3 protein and as a consequence a gain-of-NOTCH3 function [17]. This is possible since there is a degree of ligand independent activation of NOTCH3 [1, 10, 18–20].

In an effort to understand the mechanisms responsible for LMS, we created a mouse model reproducing the functional aspects of the mutations found in subjects affected by the disease [10]. In this model, termed *Notch3*^{em1Ecan} or *Notch3*$^{tm1.1Ecan}$, a tandem termination codon was introduced into exon 33 of *Notch3* causing the translation of a truncated NOTCH3 protein lacking the PEST domain. *Notch3*^{em1Ecan} mice exhibit osteopenia due to an increase in osteoclast number despite the fact that *Notch3* mRNA is not detected in the myeloid/osteoclast lineage [10]. We attributed the enhanced osteoclastogenesis to an induction of RANKL by cells of the osteoblast lineage, particularly osteocytes since they are a critical source of RANKL and as such influence bone remodeling [21, 22]. The cell responsible for the LMS phenotype could not be established with certainty since *Notch3*^{em1Ecan} are global mutant mice. Whereas the osteocyte may be the cell responsible, *Notch3* is expressed by

mural vascular cells and NOTCH3 expressed in smooth muscle cells and vessels present in the bone microenvironment could influence the skeletal phenotype of LMS [23–25].

In the present study, a conditional by inversion (COIN) approach was applied to create a conditional mouse model of LMS (*Notch3*^{COIN} or *Notch3*^{em2Ecan}) [26, 27]. The model was designed to introduce a premature STOP codon into exon 33 of *Notch3* following Cre-mediated recombination leading to the translation of a truncated NOTCH3 protein lacking the PEST domain and mimicking the genetic defect associated with LMS. To study the consequences of the NOTCH3 truncation in osteocytes, smooth muscle and endothelial cells, *Notch3*^{COIN} mice were crossed with transgenics expressing Cre recombinase under the control of the dentin matrix protein 1 (*Dmp1*), the smooth muscle protein 22 alpha (*Sm22a*) or the VE Cadherin (*Cdh5*) promoter, respectively [28–30]. Mutant and control mice were examined for skeletal phenotypic changes by microcomputed tomography (μCT).

2. MATERIALS AND METHODS

2.1 Creation of the Notch3^{COIN} Mouse Model

To generate a conditional allele of *Notch3* modeling the LMS mutation, we used a *Notch3 COIN* vector. This vector consists of rabbit β-globin (*Rbg*) intron 2 sequence with a *COIN* module introduced into exon 33 of *Notch3* in the anti-sense orientation immediately upstream of the PEST domain at nucleotide 6667 splitting exon 33 into two exons, with 4.5 kilobase (kb) 5’ and 1.5 kb 3’ homology arms, (Figure 1). In the sense orientation the *COIN* module is comprised of a gene cassette with *lox66* upstream an *Rbg* splice acceptor, human influenza hemagglutinin (HA) coding sequence with a termination codon and an GTX internal ribosome entry site and enhanced green fluorescent protein (eGFP), *Rbg* polyA and a *lox71* in an opposite orientation as that of *lox66* [26, 31]. Cre recombination results in the inversion of the *COIN* sequence placing it in the sense orientation with HA in frame with *Notch3* and resulting in a *Notch3* allele encoding a bicistronic message comprised of *Notch3ΔPEST-HA*, 2223 amino acids of NOTCH3 tagged with HA and lacking the PEST domain. Clustered regularly interspaced short palindromic repeats (CRISPR)/Cas9 technology was used to create a double-strand DNA break in *Notch3* exon 33 and introduce the *Notch3COIN* between nucleotide 6666 and 6667 of *Notch3* by homology-directed repair. The database http://crispor.tefor.net was used to scan *Notch3* sequences to identify high score target sites for potential single guide (sg) RNA. *Notch3* sgRNA 5’- CTA CTG CGG GTT CCT GCT GC was selected because of its high score and limited probabilities of off-target effects and was designed for Cas9 to cleave exon 33 of *Notch3* adjacent to a protospacer adjacent motif (PAM) positioned at nucleotide 6664 to 6666. The DNA donor and *Notch3* sgRNA/Cas9 ribonucleoprotein (RNP) complex were co-injected directly into the pronucleus of C57BL/6J one-cell embryos [32–34]. Injected embryos were transferred into CD1 pseudo-pregnant foster females, and potential founders were screened for the presence of the *COIN* module by polymerase chain reaction (PCR) and positive pups were screened for proper targeting by nested long-range PCR for founder identification. Founders were bred with wild type C57BL/6J mice and F1 pups were screened by nested long-range PCR to confirm their identity. Two live founders were generated and crossed with C57BL/6J mice to establish *Notch3*^{COIN} (syn *Notch3*^{em2Ecan}) lines.

2.2 Induction of the LMS Mutation in the Germ line, Osteocytes and Vascular Cells

To achieve the systemic inversion of the *Notch3*^{COIN} allele, F1 heterozygous *Notch3*$^{COIN/WT}$ (*Notch3*^{em2Ecan}) male mice were bred with female mice expressing Cre under the control of the *Hprt* promoter (*Hprt*^{Cre}) (*Hprt*$^{tm1(CAG-cre)Mnn}$/J, Jackson Laboratory 004302) [35]. This resulted in the germ line inversion of the *COIN* module and consequent creation of mice heterozygous for the *Notch3*^{INV} allele and termed *Notch3*$^{em2.1Ecan}$. The latter were crossed with wild type C57BL/6J mice to generate *Notch3*$^{INV/WT}$ experimental and wild type controls for study. To induce inversion of the *COIN* module in osteocytes, C57BL/6J mice harboring a transgene, where the Cre recombinase is cloned downstream of a 9.6 kb murine *Dmp1* promoter fragment (*Dmp1-Cre*) (Tg(Dmp1-cre)1Jqfe/BwdJ, Jackson 023047) were used [28]. To invert the COIN allele in smooth muscle cells, C57BL/6J mice harboring a transgene where the Cre recombinase coding sequence is driven by a 2.8 kb of murine *Sm22a* or transgelin sequences (*Sm22a-Cre* or *Tagln-Cre*, Jackson Laboratory, B6.Cg-Tg(Tagln-cre)1Her/J, 017491) were used [29]. To induce the inversion of the COIN allele in endothelial cells, C57BL/6J mice harboring a transgene where the Cre recombinase coding sequence is driven by a 2.5 kb fragment of the murine VE Cadherin (*Cdh5*)-*Cre*, Jackson Laboratory, B6.FVB-Tg(Cdh5-cre)7Mlia/J, 006137) promoter were used [30].

Hemizygous *Dmp1*, *Sm22a* or *Cdh5* Cre transgenics homozygous for the *Notch3*^{COIN} allele (*Cre*$^{+/-}$;*Notch3*$^{COIN/COIN}$) were crossed with *Notch3*$^{COIN/COIN}$ mice to generate *Cre*$^{+/-}$;*Notch3*$^{INV/INV}$ and *Notch3*$^{COIN/COIN}$ littermate controls (Figure 1). Allelic composition was determined by PCR analysis of tail DNA with specific primers, and inversion of the *COIN* module was documented by PCR analysis in DNA from tails (*Notch3*$^{em2.1Ecan}$), tibiae or aorta (*Notch3*^{em2Ecan}) (all primers were from Integrated DNA Technologies (IDT), Coralville, IA; Table 1).

Studies were approved by the Institutional Animal Care and Use Committee of UConn Health.

2.3 Microcomputed Tomography (μCT)

Femoral microarchitecture was determined using a μCT instrument (Scanco μCT 40, Scanco Medical AG, Bassersdorf, Switzerland), which was calibrated at periodic intervals with a manufacturer provided phantom [36, 37]. Femurs and vertebrae from control and experimental mice were scanned in 70% ethanol at high resolution, energy level of 55 peak kilovoltage (kVp), intensity of 145 μA, and integration time of 200 ms as reported [7, 10]. For cancellous microarchitecture, 160 slices at the distal femoral metaphysis or ~500 slices of L3 were acquired at an isotropic voxel size of 216 μm^3 and a slice thickness of 6 μm and chosen for analysis. Cancellous bone volume fraction (bone volume/total volume) and microarchitecture were evaluated starting ~1.0 mm proximal from the femoral condyles. For L3, the vertebral body was scanned in its entirety. Contours were manually drawn every 10 slices, a few voxels away from the endocortical boundary, to define the region of interest for analysis, whereas the remaining slice contours were iterated automatically. Total volume, bone volume, bone volume fraction, trabecular thickness, trabecular number, connectivity density, structure model index (SMI), and material density were measured in trabecular regions using a Gaussian filter ($\sigma = 0.8$) and defined thresholds. A threshold of 240 permil

equivalent to 355.5 mg of hydroxyapatite was used [36, 37]. For analysis of cortical bone, contours were iterated across 100 slices along the cortical shell of the femoral midshaft, excluding the marrow cavity. Analysis of bone volume/total volume, porosity, cortical thickness, total cross-sectional and cortical bone area, segmented bone area, periosteal and endosteal perimeter, and material density were conducted using a Gaussian filter ($\sigma = 0.8$, support = 1) with thresholds of 390 or 400 permil equivalent to 682.9 or 704.7mg of hydroxyapatite/cm^3, respectively.

2.4 Bone Histomorphometry

For cancellous bone histomorphometric analysis, femurs were dissected, fixed in 70% ethanol and embedded in methyl methacrylate. Femurs were sectioned at a thickness of 5 μm along the sagittal plane on a Microm microtome (Richards-Allan Scientific, Kalamazoo, MI), and stained with 0.1% toluidine blue. Parameters of bone morphometry were measured in a defined area between 0.35 mm and 2.16 mm from the growth plate at a magnification of 100x using an OsteoMeasure morphometry system (Osteometrics, Atlanta, GA). Stained sections were used to draw bone tissue and to measure trabecular separation, number and thickness, osteoid and eroded surface, as well as to count osteoblast and osteoclast number [38]

2.5 Osteocyte-enriched Cell Preparations

Osteocyte-enriched cells were obtained from *Dmp1-Cre;Notch3*$^{INV/INV}$ and *Notch3*$^{COIN/COIN}$ control mice following a modification of a previously described method [5, 39]. Femurs or tibiae were removed aseptically from experimental and control mice, dissected free from surrounding tissues, the proximal epiphyseal end was excised, and the bone marrow was removed by centrifugation. The distal epiphysis was excised, and bones were digested for 20 min at 37 °C with type II bacterial collagenase pretreated with *N*-α-tosyl-l-lysyl-chloromethyl ketone hydrochloride and subsequently exposed to 5 mM EDTA for 20 min at 37 °C. The resulting osteocyte-enriched cortical bones from experimental and control mice were cultured for 72 hours in Dulbecco Modified Medium (DMEM) supplemented with 10% fetal bovine serum prior to RNA extraction [5, 40].

2.6 Quantitative Reverse Transcription–Polymerase Chain Reaction (qRT-PCR)

Total RNA was extracted with the micro RNeasy kit (Qiagen, Valencia, CA), in accordance with manufacturer's instructions, as previously reported [7, 10, 41, 42]. Equal amounts of RNA were reverse transcribed using the iScript RT-PCR kit (Bio-Rad) and amplified in the presence of specific primers (IDT) (Table 2) with SsoAdvanced Universal SYBR Green Supermix (Bio-Rad) at 60 °C for 35 cycles. Transcript copy number was estimated by comparison with a serial dilution of cDNA for *Alpl* (encoding for alkaline phosphatase from American Type Tissue Culture Collection (ATCC), Manassas, VA), *Bglap* (encoding for osteocalcin from J. Lian, University of Vermont), *Sost* (from Thermo Fisher Scientific, Waltham, MA), *Tnfsf11* (encoding for RANKL from Source BioScience, Nottingham, UK), *Tnfrsf11b* (encoding for osteoprotegerin from ATCC), or *Notch3*^{PEST} (U. Lendahl, Addgene #47618, Watertown, MA) [43]. *Notch3*^{INV} or *Notch3*$^{\Delta PEST}$ copy number was estimated by comparison to a serial dilution of ~100 base pair synthetic DNA fragment (IDT) containing *HA* sequences that are only detectable in the inverted allele, and cloned into pcDNA3.1

(−) (Thermo Fisher Scientific, Waltham, MA). Amplification reactions were conducted in a CFX96 qRT-PCR detection system (Bio-Rad), and fluorescence was monitored during every PCR cycle at the annealing step. Data are expressed as copy number corrected for *Rpl38* (from ATCC) [44].

2.7 Statistics

Data are expressed as means ± SD. All data represent biological replicates. qRT-PCR values were derived from two technical replicates of biological replicates as indicated in the text and legends. Statistical differences were determined by unpaired Student's *t*-test for pairwise comparisons or by two-way analysis of variance for multiple comparison with Holm-Šidák post-hoc analysis using GraphPad Prism version 9.3.1 for Mac OS, GraphPad Software (San Diego, CA).

3. RESULTS

3.1 Generation of a Conditional LMS Mouse Model

To introduce the LMS mutation into selected cell populations, *Notch3*^{COIN} mice were created by inserting an artificial *COIN* intron into exon 33 of the murine *Notch3* locus and were termed *Notch3*^{em2Ecan} (Figure 1). Prior to Cre recombination the *COIN* module, a gene trap-like *lox66_HA-egfp-polyA_lox71* cassette placed in the antisense orientation, is removed by splicing of the precursor mRNA to generate a *Notch3*^{COIN} transcript that is indistinguishable from the *Notch3*^{WT} mRNA (Figure 1). In the presence of the Cre recombinase, which recognizes the *lox71* and *lox66* mutant sites in a mirror image configuration, the *lox66_HA-egfp-polyA_lox71* cassette is brought into the sense strand, causing the irreversible conversion of the *COIN* allele. The resulting allele encodes for a message that is translated into an HA-tagged NOTCH3 mutant lacking the PEST domain (Figure 1). This allele was termed *Notch3*^{INV}. The proper integration of the *COIN* module in the *Notch3*^{em2Ecan} mouse model was verified by sequencing of PCR products of the 5' and 3' arms of the vector used in founder and F1 mice. In addition, heterozygous crosses of *Notch3*^{em2Ecan} mice generated a homozygous offspring documenting loss of wild type alleles.

3.2 Inversion of the Notch3^{COIN} Allele in the Germ line Causes Osteopenia

To validate the *Notch3*^{em2Ecan} (*Notch3*^{COIN}) mouse as a model of LMS, the skeletal phenotype of *Notch3*^{INV} mice created by inversion of the *COIN* module in the germ line was determined. To this end, *Notch3*$^{COIN/WT}$ male mice were crossed with *Hprt-Cre* female mice to create *Notch3*$^{INV/WT}$ mice, and these were termed *Notch3*$^{em2.1Ecan}$. Heterozygous *Notch3*$^{em2.1Ecan}$ mice were crossed with wild type mice to create *Notch3*$^{em2.1Ecan}$ heterozygous and control wild type littermates for study. *COIN* inversion was documented by the presence of the *Notch3*^{INV} allele in DNA from tails of *Notch3*$^{em2.1Ecan}$ mice, and qRT-PCR analysis of total RNA from calvariae confirmed the expression of the *Notch3*$^{\Delta PEST}$ transcript, expressing the HA tag, in mutant mice but not in control littermates (Figure 2).

One month old heterozygous *Notch3*$^{em2.1Ecan}$ male and female mice appeared normal, albeit a small not significant reduction in weight was observed in male and femoral length was noted in female mice. μCT analysis of the distal femur revealed a 45% decrease in trabecular bone volume/total volume in 1 month old *Notch3*$^{em2.1Ecan}$ mice of both sexes (Table3, Figure 2). The decrease was secondary to a reduced number of trabeculae and to a lesser extent to a decrease in trabecular thickness. Connectivity density was lower and SMI was higher in *Notch3*$^{em2.1Ecan}$ mice than in controls, indicating a prevalence of rod-like trabeculae (Table 3, Figure 2). *Notch3*$^{em2.1Ecan}$ mice had a decrease in cortical bone area and a non-significant decrease in periosteal perimeter suggesting smaller bones. Bone histomorphometry of 1 month old *Notch3*$^{em2.1Ecan}$ mice confirmed the decrease in bone volume and trabecular number, but did not reveal changes in osteoblast number, osteoclast number or eroded surface (Table 4). The results are consistent with the phenotype reported for global *Notch3LMS* mutant (*Notch3*^{em1Ecan}) mice, and validate the *Notch3*^{COIN} mouse as a model to study the contribution of selected cell lineages to the phenotype [10].

3.3 Inversion of the Notch3^{COIN} Allele in Osteocytes Causes Osteopenia

Because *Notch3* is preferentially expressed by osteocytes, we wished to determine whether the osteopenia observed in *Notch3*^{em1Ecan} LMS global mutant mice was driven by an effect in cells of the osteocytic lineage [3, 5]. For this purpose, *Dmp1-Cre*;*Notch3*$^{COIN/COIN}$ (*Notch3*^{em2Ecan}) were crossed with *Notch3*$^{COIN/COIN}$ mice to create *Dmp1-Cre*;*Notch3*$^{INV/INV}$ mice and littermate *Notch3*$^{COIN/COIN}$ controls. Inversion of the *COIN* allele was detected in DNA from tibiae of *Dmp1-Cre*;*Notch3*$^{INV/INV}$ mice but not in littermate controls (Figure 3). Accordingly, the *Notch3*$^{\Delta PEST}$ transcript was detected only in calvariae from *Dmp1-Cre*;*Notch3*$^{INV/INV}$ mice, documenting the induction of the mutation in cells that express *Dmp1*.

The general appearance, weight and femoral length of 1 month old *Dmp1-Cre*;*Notch3*$^{INV/INV}$ mice were not different from those of control sex-matched littermates (Figure 3). At 1 month of age, μCT revealed significant cancellous bone osteopenia in *Dmp1-Cre*;*Notch3*$^{INV/INV}$ male mice; this was associated with decreased connectivity density and increased SMI (both $p < 0.05$ by unpaired *t*-test; $p > 0.05$ by ANOVA), indicating a prevalence of rod-like over plate-like trabeculae (Table 5, Figure 3). Cortical bone and female mice were not affected. The cancellous bone osteopenic phenotype was confirmed in vertebral (L3) bone of male 1 month old *Dmp1-Cre;Notch3*$^{INV/INV}$ mice. Bone volume/total volume was decreased from (means ± SD; n = 4 to 5) 13.0 ± 0.6 in control *Notch3*$^{COIN/COIN}$ to 11.1 ±0.4 in *Dmp1-Cre;Notch3*$^{INV/INV}$ mice ($p < 0.05$ by unpaired *t*-test; $p > 0.05$ by ANOVA). Bone histomorphometric analysis of 1 month old male *Dmp1-Cre;Notch3*^{INV} mice did not reveal changes in osteoblast or osteoclast number compared to control sex-matched *Notch3*^{COIN} mice (data not shown).

3.4 Inversion of the Notch3^{COIN} Allele Induces Tnfsf11 but does not Change Alpl, Bglap or Sost Expression

To determine possible mechanisms responsible for the skeletal phenotype of the *Dmp1-Cre*;*Notch3*$^{INV/INV}$ mice, osteocyte-enriched preparations were obtained from tibiae of *Dmp1-Cre;Notch3*$^{INV/INV}$ and control *Notch3*$^{COIN/COIN}$ littermates. *Tnfsf11* (encoding

RANKL) was induced in osteocytes from *Dmp1-Cre*;*Notch3*$^{INV/INV}$ mice, whereas the expression of *Tnfrsf11b* (encoding osteoprotegerin) was not changed (Figure 4).

To ascertain whether there were possible changes in osteoblast/osteocyte function in *Notch3*^{INV} mice, calvariae from *Notch3*$^{2.1Ecan}$ (germline inverted) and *Dmp1-Cre;Notch3*$^{INV/INV}$ were extracted and examined for gene expression. There were no significant differences between control and experimental mice in *Alpl*, *Bglap* or *Sost* mRNA levels (all values copy number/*Rpl38*; means ± SD; n = 10 – 11). *Alpl* 2.1 ± 0.2 in wild type and 1.6 ± 0.2 in *Notch3*$^{2.1Ecan}$ mice, *Bglap* 11.9 ± 1.2 in wild type and 9.5 ± 0.8 in *Notch3*$^{2.1Ecan}$ mice (both $p > 0.05$), and *Sost* 2.8 ± 0.3 in wild type and 2.0 ± 0.2 in *Notch3*$^{2.1Ecan}$ mice ($p < 0.053$). *Alpl* 1.2 ± 0.1 in control and 1.3 ± 0.1 in *Dmp1-Cre;Notch*$^{INV/INV}$ mice, *Bglap* 6.4 ± 0.9 in control and 7.7 ± 1.8 in *Dmp1-Cre;Notch3*$^{INV/INV}$, and *Sost* 2.2 ± 0.3 in control and 1.9 ± 0.3 in *Dmp1-Cre;Notch3*$^{INV/INV}$ mice (all $p > 0.05$).

3.5 Inversion of the Notch3^{COIN}Allele in Vascular Cells does not Cause Osteopenia

Because NOTCH3 is the prevalent Notch receptor expressed in mural vascular cells, we asked whether the activation of the *Notch3LMS* mutation in vascular cells could be responsible for the osteopenic phenotype [24, 25, 45]. To this end, *Sm22a-Cre;Notch3*$^{COIN/COIN}$ mice were crossed with *Notch3*$^{COIN/COIN}$ to introduce the *Notch3LMS* mutation in smooth muscle cells. One month old *Sm22a-Cre;Notch3*$^{INV/INV}$ mice appeared normal, and their weight and femoral length were not different from control *Notch3*$^{COIN/COIN}$ mice (Figure 5). Inversion of the COIN allele was documented in DNA from the aorta of *Sm22a-Cre;Notch3*$^{INV/INV}$ mice and inversion did not occur in control mice. Accordingly, *Notch3*$^{\Delta PEST}$ transcripts were detected in aorta from *Sm22a-Cre;Notch3*$^{INV/INV}$ mice. Although a modest degree of inversion of the COIN allele was detected in tibiae from *Sm22a-Cre;Notch3*$^{INV/INV}$ mice, there was no induction of *Notch3*$^{\Delta PEST}$ transcript in this tissue indicating that the mutant transcript was not expressed in the bone environment. Accordingly, cancellous and cortical bone architecture revealed no differences between 1 month old *Sm22a-Cre;Notch3*$^{INV/INV}$ mice and control littermates (Table 6).

Although *Notch3* is not expressed or expressed at very low levels in endothelial cells, Notch activation in endothelial cells can influence bone remodeling and NOTCH3 activity in mural cells [23, 25]. To determine whether the introduction of the *Notch3LMS* mutation in endothelial cells caused or did not cause a skeletal phenotype, *Cdh5-Cre;Notch3*$^{COIN/COIN}$ mice were crossed with *Notch3*$^{COIN/COIN}$ to induce *Notch3* COIN inversion in endothelial cells. One month old *Cdh5-Cre;Notch3*$^{INV/INV}$ mice appeared normal, and their weight and femoral length were not substantially different from controls (Figure 6). Cre-mediated inversion of the COIN allele was documented in aorta and tibiae, and low levels of *Notch3*$^{\Delta PEST}$ mRNA were detected in tibiae but not in aorta from *Cdh5-Cre;Notch3*$^{INV/INV}$ mice. Copy number revealed that the expression of *Notch3*$^{\Delta PEST}$ transcripts was 1/100 the one observed in bones from *Notch3*$^{em2.1Ecan}$ (germline inverted) mice and *Dmp1-Cre;Notch3*$^{INV/INV}$ mice. The modest induction of *Notch3*$^{\Delta PEST}$ in tibiae was possibly due to the presence of small vessels in the bone environment, and bone microarchitecture

was not different between 1 month old *Cdh5-Cre;Notch3*$^{INV/INV}$ and *Notch3*^{em2Ecan} control littermate mice (Table 7).

4. DISCUSSION

In previous studies, we have shown that a mouse model harboring a *Notch3* mutation reproducing the functional outcomes of LMS exhibits osteopenia [10]. However, the cell responsible for the phenotype was not identified because the model used harbors the *Notch3* mutation in all cell lineages. The establishment of the cell responsible for the phenotype is of particular interest in the case of NOTCH3 since its transcript expression is not detected in the myeloid/osteoclast lineage [3]. Instead, *Notch3* is mostly expressed in osteocytes and mural vascular cells [3, 5, 24]. The present study, aimed at establishing the contributions of specific cell lineages to the LMS skeletal phenotype. This was possible by the creation of a COIN mouse model termed *Notch3*^{em2Ecan}.

The pathogenic variants associated with LMS occur within exon 33 of *NOTCH3*, and the conditional insertion of a premature STOP codon in the homologous region of the murine *Notch3* locus was achieved by the creation of a *COIN* allele. The *COIN* module was introduced without disrupting the expression or function of the targeted allele under basal conditions, and this would not be possible with traditional Cre-*loxP* approaches [26]. *Notch3*$^{em2.1Ecan}$ mutants of both sexes, generated by germ line inversion of the *COIN* module, exhibited cancellous and cortical bone osteopenia phenocopying *Notch3*^{em1Ecan} global LMS mutants and validating the *Notch3*^{COIN} approach.

Selective introduction of the LMS mutation in osteocytes led to osteopenia, albeit this was modest and restricted to male mutant mice since female mice were not affected. Although *Dmp1* is preferentially expressed by osteocytes, *Dmp1* promoter activity is also detected in mature osteoblasts, so that the osteopenic phenotype observed is secondary to an effect in both cells [46, 47]. The bone loss occurred mostly at femoral sites. Although an increased expression of RANKL without a concomitant alteration in osteoprotegerin expression was found in osteocytes from *Dmp1-Cre;Notch3*$^{INV/INV}$ mice, bone histomorphometry did not reveal an increase in osteoclast number. Osteocyte-derived RANKL plays a pivotal role in bone remodeling, but other mechanisms could have played a role in the phenotype [21, 48, 49]. Since *Dmp1* is expressed in mineralized tissues during development, it is possible that the phenotype of *Dmp1-Cre;Notch3*$^{INV/INV}$ was due to effects of NOTCH3 during skeletal development [50]. It is important to mention that mice of both sexes displayed osteopenia in the global *Notch3*^{em1Ecan} mouse model, and following the germline inversion of *Notch3*^{em2Ecan} conditional mutants. There is no apparent explanation for the sex dimorphism of the *Dmp1-Cre;Notch3*$^{INV/INV}$ skeletal phenotype, and there was no evidence of less efficient Cre recombination in osteocytes from female than from male mice. This dimorphism was also noted when exploring the effects of the Notch ligand Delta-like 4 (DLL4) in bone, and female mice were more resistant to the actions of DLL4 and this was attributed to their lower bone surface [51]. The sexual dimorphism also could be related to a higher rate of bone remodeling in young female than in male mice, a characteristic of the C57BL/6J genetic background [37]. It is important to note that the number of osteocytes is not substantially different in bones from male and female young C57BL/6J mice, so that the

expression of *Dmp1* would be expected to be similar in both sexes [40]. Estrogens induce the Notch ligand JAGGED 1 (JAG1) and NOTCH1 in breast cancer MCF7 endothelial cells and bone marrow stromal cells and as a consequence activate Notch signaling [52, 53]. This would suggest that the lack of a phenotype in female mice is not related to an estrogen effect, which would be expected to amplify the Notch signal. Evidence of an estrogen effect on Notch signaling *in vivo* is less compelling [54].

Although the skeletal phenotype of *Dmp1-Cre;Notch3*$^{INV/INV}$ male mice mirrors the phenotype of global *Notch3*^{em1Ecan} mice and of germ line inverted *Notch3*$^{em2.1Ecan}$ mice, it is of a more modest nature. This may relate to insufficient recombination in osteocytes/osteoblasts or may indicate that other cells harboring the *Notch3* LMS mutation contribute to the osteopenic phenotype.

In contrast to the direct actions of NOTCH1 and NOTCH2 on osteoclast cell differentiation, NOTCH3 has distinct and indirect effects in the myeloid lineage, since it is not expressed in these cells [3, 10]. NOTCH3 induces osteoclastogenesis only by indirect mechanisms and previous work in cells from global *Notch*^{em1Ecan} mice demonstrated enhanced osteoclastogenesis in co-cultures of bone marrow derived macrophages from wild type mice with osteoblasts from *Notch3*^{em1Ecan} mice. This suggested that the cell responsible for the *Notch3*^{em1Ecan} phenotype was of the osteoblast lineage, possibly by increasing the expression of RANKL. This could have important therapeutic implications in individuals with LMS and bone loss, which could be ameliorated by the administration of anti-RANKL antibodies, such a denosumab. This has been the case for the related disorder, Hajdu Cheney Syndrome, which is associated with *NOTCH2* mutations and a NOTCH2 gain of function [55, 56].

The skeleton contains various types of mural and endothelial cells that play an important role in osteogenesis, hematopoiesis and vascular homeostasis and endothelial cells are the most important secretory cells in the bone environment [57–59]. Activation of Notch signaling in endothelial cells promotes angiogenesis and osteogenesis, whereas the inactivation of *Rbpjk* or *Dll4*, and consequent decline in Notch canonical signaling in endothelial cells results in impaired angiogenesis and bone loss [59]. However, the induction of the *Notch3LMS* mutation in *Cdh5*-expressing cells did not result in a skeletal phenotype. This is most likely related to the low level or no expression of *Notch3* in endothelial cells [60]. *Notch3* is expressed in vascular smooth muscle cells where it plays a critical role in blood vessel wall integrity [60–62]. The induction of the *Notch3LMS* mutation in *Sm22a* smooth muscle-expressing cells did not cause a skeletal phenotype [63]. However, *Notch3*$^{\Delta PEST}$ transcripts were not detected in tibiae of *Sm22a-Cre;Notch3*$^{INV/INV}$ mice possibly because the expression of Sm22a is limited to mural vascular cells not present in the bone environment and explaining the absence of the skeletal phenotype. This does not exclude a role of NOTCH3 in the structure of mural vessels, it simply indicates that smooth muscle vascular NOTCH3 does influence bone remodeling.

Limitations of this work include: 1) The efficiency of the various Cre drivers used in the bone environment was not equal and could have contributed to differences in the phenotype. To assess Cre-dependent activity, we determined *Notch3*$^{\Delta PEST}$ transcripts

expressed only after recombination. *Notch3*$^{\Delta PEST}$ was not detected in bones from *Sm22a-Cre;Notch3*$^{INV/INV}$ mice and copy number in *Cdh5-Cre;Notch3*$^{INV/INV}$ was about 100 times lower than in bone from *Dmp1-Cre;Notch3*$^{INV/INV}$ mice indicating different levels of Cre recombination efficiency, at least in bone, possibly explaining the different phenotypes; 2) *Cre;Notch3*$^{INV/INV}$ mice were compared to Cre negative *Notch3*$^{COIN/COIN}$ littermates and no additional controls, such as wild type mice were utilized for comparison; 3) The phenotype was established in young mice prior to the attainment of skeletal maturity and the phenotype could be secondary to developmental events and might not persist at maturity; and 4) The mechanisms responsible for the osteopenia of *Hprt-Cre;Notch3*$^{INV/WT}$ and *Dmp1-Cre;Notch3*$^{INV/INV}$ mice were not elucidated.

5. CONCLUSIONS

In conclusion, expression of a *Notch3* mutant lacking the PEST domain and mimicking LMS in osteocytes causes osteopenia in male mice.

ACKNOWLEDGMENTS

The authors thank Magda Mocarska for technical assistance and Mary Yurczak for secretarial support.

FUNDING

This work was supported by the National Institute of Arthritis and Musculoskeletal and Skin Diseases [AR072987] (EC). The content is solely the responsibility of the authors and does not necessarily represent the official views of the National Institutes of Health.

ABBREVIATIONS

bp	base pair
cadh5	VE Cadherin
CRISPR	clustered regularly interpersonal short palindromic repeats
COIN	conditional by inversion
Dmp1	dentin matrix protein 1
DMEM	Dulbecco Modified Medium
eGFP	enhanced green fluorescent protein
kVp	kilovoltage
HA	hemagglutinin
kb	kilobase
LMS	Lateral Meningocele Syndrome
μCT	microcomputed tomography
PCR	polymerase chain reaction

pA	polyadenylation signal
PEST	proline (P), glutamic acid (E), serine (S) and threonine (T) domain
PAM	protospacer adjacent motif
qRT-PCR	quantitative reverse transcript-polymerase chain reaction
Rbg	rabbit β-globin
RANKL	receptor activator of nuclear factor-κB ligand
RNA-Seq	RNA sequencing
RNP	ribonucleoprotein
sg	single guide
Sm22a	smooth muscle protein 22 alpha
SMI	structure model index

REFERENCES

[1]. Siebel C, Lendahl U, Notch Signaling in Development, Tissue Homeostasis, and Disease, Physiol. Rev 97(4) (2017) 1235–1294. 10.1152/physrev.00005.2017 [PubMed: 28794168]

[2]. Zanotti S, Canalis E, Notch Signaling and the Skeleton, Endocr. Rev 37(3) (2016) 223–253. 10.1210/er.2016-1002 [PubMed: 27074349]

[3]. Canalis E, Notch in skeletal physiology and disease, Osteoporos.Int 29(12) (2018) 2611–2621. 10.1007/s00198-018-4694-3 [PubMed: 30194467]

[4]. Bai S, Kopan R, Zou W, Hilton MJ, Ong CT, Long F, Ross FP, Teitelbaum SL, NOTCH1 regulates osteoclastogenesis directly in osteoclast precursors and indirectly via osteoblast lineage cells, J. Biol. Chem 283(10) (2008) 6509–6518. [PubMed: 18156632]

[5]. Zanotti S, Canalis E, Parathyroid hormone inhibits Notch signaling in osteoblasts and osteocytes, Bone 103 (2017) 159–167. 10.1016/j.bone.2017.06.027 [PubMed: 28676438]

[6]. Fukushima H, Nakao A, Okamoto F, Shin M, Kajiya H, Sakano S, Bigas A, Jimi E, Okabe K, The association of Notch2 and NF-kappaB accelerates RANKL-induced osteoclastogenesis, Mol. Cell Biol 28(20) (2008) 6402–6412. [PubMed: 18710934]

[7]. Canalis E, Schilling L, Yee SP, Lee SK, Zanotti S, Hajdu Cheney Mouse Mutants Exhibit Osteopenia, Increased Osteoclastogenesis and Bone Resorption, J. Biol. Chem 291 (2016) 1538–1551. 10.1074/jbc.M115.685453 [PubMed: 26627824]

[8]. Canalis E, Parker K, Feng JQ, Zanotti S, Osteoblast Lineage-specific Effects of Notch Activation in the Skeleton, Endocrinology 154(2) (2013) 623–634. en.2012–1732 [pii];10.1210/en.2012-1732 [doi] [PubMed: 23275471]

[9]. Yu J, Canalis E, The Hajdu Cheney mutation sensitizes mice to the osteolytic actions of tumor necrosis factor alpha, J. Biol. Chem 294(39) (2019) 14203–14214. 10.1074/jbc.RA119.009824 [PubMed: 31371452]

[10]. Canalis E, Yu J, Schilling L, Yee SP, Zanotti S, The lateral meningocele syndrome mutation causes marked osteopenia in mice, J. Biol. Chem 293(36) (2018) 14165–14177. 10.1074/jbc.RA118.004242 [PubMed: 30042232]

[11]. Yu J, Canalis E, Notch and the regulation of osteoclast differentiation and function, Bone 138 (2020) 115474. 10.1016/j.bone.2020.115474 [PubMed: 32526405]

[12]. Takayanagi H, Kim S, Koga T, Nishina H, Isshiki M, Yoshida H, Saiura A, Isobe M, Yokochi T, Inoue J, Wagner EF, Mak TW, Kodama T, Taniguchi T, Induction and activation of the

transcription factor NFATc1 (NFAT2) integrate RANKL signaling in terminal differentiation of osteoclasts, Dev. Cell 3(6) (2002) 889–901. [PubMed: 12479813]

[13]. Tsukasaki M, Takayanagi H, Osteoimmunology: evolving concepts in bone-immune interactions in health and disease, Nat. Rev. Immunol 19(10) (2019) 626–642. 10.1038/s41577-019-0178-8 [PubMed: 31186549]

[14]. Lehman RA, Stears JC, Wesenberg RL, Nusbaum ED, Familial osteosclerosis with abnormalities of the nervous system and meninges, J. Pediatr 90(1) (1977) 49–54. [PubMed: 830893]

[15]. Gripp KW, Scott CI Jr., Hughes HE, Wallerstein R, Nicholson L, States L, Bason LD, Kaplan P, Zderic SA, Duhaime AC, Miller F, Magnusson MR, Zackai EH, Lateral meningocele syndrome: three new patients and review of the literature, Am. J. Med. Genet 70(3) (1997) 229–239. [PubMed: 9188658]

[16]. Avela K, Valanne L, Helenius I, Makitie O, Hajdu-Cheney syndrome with severe dural ectasia, Am. J. Med. Genet. A 155A(3) (2011) 595–598. 10.1002/ajmg.a.33510 [doi] [PubMed: 21337686]

[17]. Gripp KW, Robbins KM, Sobreira NL, Witmer PD, Bird LM, Avela K, Makitie O, Alves D, Hogue JS, Zackai EH, Doheny KF, Stabley DL, Sol-Church K, Truncating mutations in the last exon of NOTCH3 cause lateral meningocele syndrome, Am. J. Med. Genet. A 167A(2) (2015) 271–281. 10.1002/ajmg.a.36863 [PubMed: 25394726]

[18]. Choy L, Hagenbeek TJ, Solon M, French D, Finkle D, Shelton A, Venook R, Brauer MJ, Siebel CW, Constitutive NOTCH3 Signaling Promotes the Growth of Basal Breast Cancers, Cancer Res. 77(6) (2017) 1439–1452. 10.1158/0008-5472.CAN-16-1022 [PubMed: 28108512]

[19]. Xu X, Choi SH, Hu T, Tiyanont K, Habets R, Groot AJ, Vooijs M, Aster JC, Chopra R, Fryer C, Blacklow SC, Insights into Autoregulation of Notch3 from Structural and Functional Studies of Its Negative Regulatory Region, Structure 23(7) (2015) 1227–1235. 10.1016/j.str.2015.05.001 [PubMed: 26051713]

[20]. Tiyanont K, Wales TE, Siebel CW, Engen JR, Blacklow SC, Insights into Notch3 activation and inhibition mediated by antibodies directed against its negative regulatory region, J. Mol. Biol 425(17) (2013) 3192–3204. 10.1016/j.jmb.2013.05.025 [PubMed: 23747483]

[21]. Xiong J, O'Brien CA, Osteocyte RANKL: New insights into the control of bone remodeling, J. Bone Miner. Res 27(3) (2012) 499–505. 10.1002/jbmr.1547 [doi] [PubMed: 22354849]

[22]. Dallas SL, Prideaux M, Bonewald LF, The osteocyte: an endocrine cell … and more, Endocr. Rev 34(5) (2013) 658–690. 10.1210/er.2012-1026 [PubMed: 23612223]

[23]. Ramasamy SK, Kusumbe AP, Wang L, Adams RH, Endothelial Notch activity promotes angiogenesis and osteogenesis in bone, Nature 507(7492) (2014) 376–380. 10.1038/nature13146 [PubMed: 24647000]

[24]. Domenga V, Fardoux P, Lacombe P, Monet M, Maciazek J, Krebs LT, Klonjkowski B, Berrou E, Mericskay M, Li Z, Tournier-Lasserve E, Gridley T, Joutel A, Notch3 is required for arterial identity and maturation of vascular smooth muscle cells, Genes Dev. 18(22) (2004) 2730–2735. 10.1101/gad.308904 [PubMed: 15545631]

[25]. Liu H, Kennard S, Lilly B, NOTCH3 expression is induced in mural cells through an autoregulatory loop that requires endothelial-expressed JAGGED1, Circ Res 104(4) (2009) 466–475. 10.1161/CIRCRESAHA.108.184846 [PubMed: 19150886]

[26]. Economides AN, Frendewey D, Yang P, Dominguez MG, Dore AT, Lobov IB, Persaud T, Rojas J, McClain J, Lengyel P, Droguett G, Chernomorsky R, Stevens S, Auerbach W, DeChiara TM, Pouyemirou W, Cruz JM Jr., Feeley K, Mellis IA, Yasenchack J, Hatsell SJ, Xie L, Latres E, Huang L, Zhang Y, Pefanis E, Skokos D, Deckelbaum RA, Croll SD, Davis S, Valenzuela DM, Gale NW, Murphy AJ, Yancopoulos GD, Conditionals by inversion provide a universal method for the generation of conditional alleles, Proc. Natl. Acad. Sci. U. S. A 110(34) (2013) E3179–E3188. 1217812110 [pii];10.1073/pnas.1217812110 [doi] [PubMed: 23918385]

[27]. Zanotti S, Yu J, Sanjay A, Schilling L, Schoenherr C, Economides AN, Canalis E, Sustained Notch2 signaling in osteoblasts, but not in osteoclasts, is linked to osteopenia in a mouse model of Hajdu-Cheney syndrome, J. Biol. Chem 292(29) (2017) 12232–12244. 10.1074/jbc.M117.786129 [PubMed: 28592489]

[28]. Lu Y, Xie Y, Zhang S, Dusevich V, Bonewald LF, Feng JQ, DMP1-targeted Cre expression in odontoblasts and osteocytes, J. Dent. Res 86(4) (2007) 320–325. [PubMed: 17384025]

[29]. Holtwick R, Gotthardt M, Skryabin B, Steinmetz M, Potthast R, Zetsche B, Hammer RE, Herz J, Kuhn M, Smooth muscle-selective deletion of guanylyl cyclase-A prevents the acute but not chronic effects of ANP on blood pressure, Proc. Natl. Acad. Sci. U. S. A 99(10) (2002) 7142–7147. 10.1073/pnas.102650499 [PubMed: 11997476]

[30]. Alva JA, Zovein AC, Monvoisin A, Murphy T, Salazar A, Harvey NL, Carmeliet P, Iruela-Arispe ML, VE-Cadherin-Cre-recombinase transgenic mouse: a tool for lineage analysis and gene deletion in endothelial cells, Dev. Dyn 235(3) (2006) 759–767. 10.1002/dvdy.20643 [PubMed: 16450386]

[31]. Canalis E, Zanotti S, Beamer WG, Economides AN, Smerdel-Ramoya A, Connective Tissue Growth Factor Is Required for Skeletal Development and Postnatal Skeletal Homeostasis in Male Mice, Endocrinology 151(8) (2010) 3490–3501. [PubMed: 20534727]

[32]. Liang X, Potter J, Kumar S, Zou Y, Quintanilla R, Sridharan M, Carte J, Chen W, Roark N, Ranganathan S, Ravinder N, Chesnut JD, Rapid and highly efficient mammalian cell engineering via Cas9 protein transfection, J. Biotechnol 208 (2015) 44–53. 10.1016/j.jbiotec.2015.04.024 [PubMed: 26003884]

[33]. Burger A, Lindsay H, Felker A, Hess C, Anders C, Chiavacci E, Zaugg J, Weber LM, Catena R, Jinek M, Robinson MD, Mosimann C, Maximizing mutagenesis with solubilized CRISPR-Cas9 ribonucleoprotein complexes, Development 143(11) (2016) 2025–2037. 10.1242/dev.134809 [PubMed: 27130213]

[34]. Paix A, Folkmann A, Rasoloson D, Seydoux G, High Efficiency, Homology-Directed Genome Editing in Caenorhabditis elegans Using CRISPR-Cas9 Ribonucleoprotein Complexes, Genetics 201(1) (2015) 47–54. 10.1534/genetics.115.179382 [PubMed: 26187122]

[35]. Tang SH, Silva FJ, Tsark WM, Mann JR, A Cre/loxP-deleter transgenic line in mouse strain 129S1/SvImJ, Genesis 32(3) (2002) 199–202. 10.1002/gene.10030 [pii] [PubMed: 11892008]

[36]. Bouxsein ML, Boyd SK, Christiansen BA, Guldberg RE, Jepsen KJ, Muller R, Guidelines for assessment of bone microstructure in rodents using micro-computed tomography, J. Bone Miner. Res 25(7) (2010) 1468–1486. [PubMed: 20533309]

[37]. Glatt V, Canalis E, Stadmeyer L, Bouxsein ML, Age-Related Changes in Trabecular Architecture Differ in Female and Male C57BL/6J Mice, J. Bone Miner. Res 22(8) (2007) 1197–1207. [PubMed: 17488199]

[38]. Dempster DW, Compston JE, Drezner MK, Glorieux FH, Kanis JA, Malluche H, Meunier PJ, Ott SM, Recker RR, Parfitt AM, Standardized nomenclature, symbols, and units for bone histomorphometry: a 2012 update of the report of the ASBMR Histomorphometry Nomenclature Committee, J. Bone Miner. Res 28(1) (2013) 2–17. 10.1002/jbmr.1805 [doi] [PubMed: 23197339]

[39]. Halleux C, Kramer I, Allard C, Kneissel M, Isolation of mouse osteocytes using cell fractionation for gene expression analysis, Methods Mol. Biol 816 (2012) 55–66. 10.1007/978-1-61779-415-5_5 [doi] [PubMed: 22130922]

[40]. Canalis E, Schilling L, Zanotti S, Effects of Sex and Notch Signaling on the Osteocyte Cell Pool, J. Cell. Physiol 232(2) (2017) 363–370. 10.1002/jcp.25433 [PubMed: 27192486]

[41]. Nazarenko I, Pires R, Lowe B, Obaidy M, Rashtchian A, Effect of primary and secondary structure of oligodeoxyribonucleotides on the fluorescent properties of conjugated dyes, Nucleic Acids Res. 30(9) (2002) 2089–2195. [PubMed: 11972350]

[42]. Nazarenko I, Lowe B, Darfler M, Ikonomi P, Schuster D, Rashtchian A, Multiplex quantitative PCR using self-quenched primers labeled with a single fluorophore, Nucleic Acids Res. 30(9) (2002) e37. [PubMed: 11972352]

[43]. Lardelli M, Williams R, Mitsiadis T, Lendahl U, Expression of the Notch 3 intracellular domain in mouse central nervous system progenitor cells is lethal and leads to disturbed neural tube development, Mech Dev 59(2) (1996) 177–190. 10.1016/0925-4773(96)00589-8 [PubMed: 8951795]

[44]. Kouadjo KE, Nishida Y, Cadrin-Girard JF, Yoshioka M, St-Amand J, Housekeeping and tissue-specific genes in mouse tissues, BMC Genomics 8 (2007) 127. 10.1186/1471-2164-8-127 [PubMed: 17519037]

[45]. Boucher J, Gridley T, Liaw L, Molecular pathways of notch signaling in vascular smooth muscle cells, Front Physiol 3 (2012) 81. 10.3389/fphys.2012.00081 [PubMed: 22509166]

[46]. Kalajzic I, Braut A, Guo D, Jiang X, Kronenberg MS, Mina M, Harris MA, Harris SE, Rowe DW, Dentin matrix protein 1 expression during osteoblastic differentiation, generation of an osteocyte GFP-transgene, Bone 35(1) (2004) 74–82. 10.1016/j.bone.2004.03.006 [doi];S8756328204001097 [pii] [PubMed: 15207743]

[47]. Couasnay G, Madel MB, Lim J, Lee B, Elefteriou F, Sites of Cre-recombinase activity in mouse lines targeting skeletal cells, J. Bone Miner. Res 36(9) (2021) 1661–1679. 10.1002/jbmr.4415 [PubMed: 34278610]

[48]. Xiong J, Onal M, Jilka RL, Weinstein RS, Manolagas SC, O'Brien CA, Matrix-embedded cells control osteoclast formation, Nat. Med 17(10) (2011) 1235–1241. nm.2448 [pii];10.1038/nm.2448 [doi] [PubMed: 21909103]

[49]. Nakashima T, Hayashi M, Fukunaga T, Kurata K, Oh-Hora M, Feng JQ, Bonewald LF, Kodama T, Wutz A, Wagner EF, Penninger JM, Takayanagi H, Evidence for osteocyte regulation of bone homeostasis through RANKL expression, Nat. Med 17(10) (2011) 1231–1234. nm.2452 [pii];10.1038/nm.2452 [doi] [PubMed: 21909105]

[50]. Feng JQ, Huang H, Lu Y, Ye L, Xie Y, Tsutsui TW, Kunieda T, Castranio T, Scott G, Bonewald LB, Mishina Y, The Dentin matrix protein 1 (Dmp1) is specifically expressed in mineralized, but not soft, tissues during development, J. Dent. Res 82(10) (2003) 776–780. [PubMed: 14514755]

[51]. Xu C, Dinh VV, Kruse K, Jeong HW, Watson EC, Adams S, Berkenfeld F, Stehling M, Rasouli SJ, Fan R, Chen R, Bedzhov I, Chen Q, Kato K, Pitulescu ME, Adams RH, Induction of osteogenesis by bone-targeted Notch activation, eLife 11 (2022) 10.7554/eLife.60183

[52]. Soares R, Balogh G, Guo S, Gartner F, Russo J, Schmitt F, Evidence for the notch signaling pathway on the role of estrogen in angiogenesis, Mol. Endocrinol 18(9) (2004) 2333–2343. 10.1210/me.2003-0362 [PubMed: 15192074]

[53]. Fan JZ, Yang L, Meng GL, Lin YS, Wei BY, Fan J, Hu HM, Liu YW, Chen S, Zhang JK, He QZ, Luo ZJ, Liu J, Estrogen improves the proliferation and differentiation of hBMSCs derived from postmenopausal osteoporosis through notch signaling pathway, Mol. Cell. Biochem 392(1–2) (2014) 85–93. 10.1007/s11010-014-2021-7 [PubMed: 24752351]

[54]. Farr JN, Roforth MM, Fujita K, Nicks KM, Cunningham JM, Atkinson EJ, Therneau TM, McCready LK, Peterson JM, Drake MT, Monroe DG, Khosla S, Effects of Age and Estrogen on Skeletal Gene Expression in Humans as Assessed by RNA Sequencing, PLoS One 10(9) (2015) e0138347. 10.1371/journal.pone.0138347 [PubMed: 26402159]

[55]. Canalis E, Clinical and experimental aspects of notch receptor signaling: Hajdu-Cheney syndrome and related disorders, Metabolism 80 (2018) 48–56. 10.1016/j.metabol.2017.08.002 [PubMed: 28941602]

[56]. Adami G, Rossini M, Gatti D, Orsolini G, Idolazzi L, Viapiana O, Scarpa A, Canalis E, Hajdu Cheney Syndrome; report of a novel NOTCH2 mutation and treatment with denosumab, Bone 92 (2016) 150–156. 10.1016/j.bone.2016.08.025 [PubMed: 27592446]

[57]. Sivaraj KK, Adams RH, Blood vessel formation and function in bone, Development 143(15) (2016) 2706–2715. 10.1242/dev.136861 [PubMed: 27486231]

[58]. Filipowska J, Tomaszewski KA, Niedzwiedzki L, Walocha JA, Niedzwiedzki T, The role of vasculature in bone development, regeneration and proper systemic functioning, Angiogenesis 20(3) (2017) 291–302. 10.1007/s10456-017-9541-1 [PubMed: 28194536]

[59]. Kusumbe AP, Ramasamy SK, Adams RH, Coupling of angiogenesis and osteogenesis by a specific vessel subtype in bone, Nature 507(7492) (2014) 323–328. 10.1038/nature13145 [PubMed: 24646994]

[60]. Liu H, Zhang W, Kennard S, Caldwell RB, Lilly B, Notch3 is critical for proper angiogenesis and mural cell investment, Circ Res 107(7) (2010) 860–870. 10.1161/CIRCRESAHA.110.218271 [PubMed: 20689064]

[61]. Henshall TL, Keller A, He L, Johansson BR, Wallgard E, Raschperger E, Mae MA, Jin S, Betsholtz C, Lendahl U, Notch3 is necessary for blood vessel integrity in the central nervous system, Arterioscler Thromb Vasc Biol 35(2) (2015) 409–420. 10.1161/ATVBAHA.114.304849 [PubMed: 25477343]

[62]. Baeten JT, Lilly B, Notch Signaling in Vascular Smooth Muscle Cells, Adv. Pharmacol 78 (2017) 351–382. 10.1016/bs.apha.2016.07.002 [PubMed: 28212801]

[63]. Li L, Miano JM, Cserjesi P, Olson EN, SM22 alpha, a marker of adult smooth muscle, is expressed in multiple myogenic lineages during embryogenesis, Circ Res 78(2) (1996) 188–195. 10.1161/01.res.78.2.188 [PubMed: 8575061]

Highlights

- Lateral Meningocele Syndrome (LMS) is associated with *NOTCH3* mutations
- A conditional by inversion (COIN) model was used to introduce *Notch3* LMS mutations
- Germline $Notch3^{COIN}$ inversion resulted in osteopenia
- Introduction of the *Notch3 LMS* mutation in osteocytes caused osteopenia
- Introduction of the *Notch3 LMS* mutation in vascular cells did no cause osteopenia

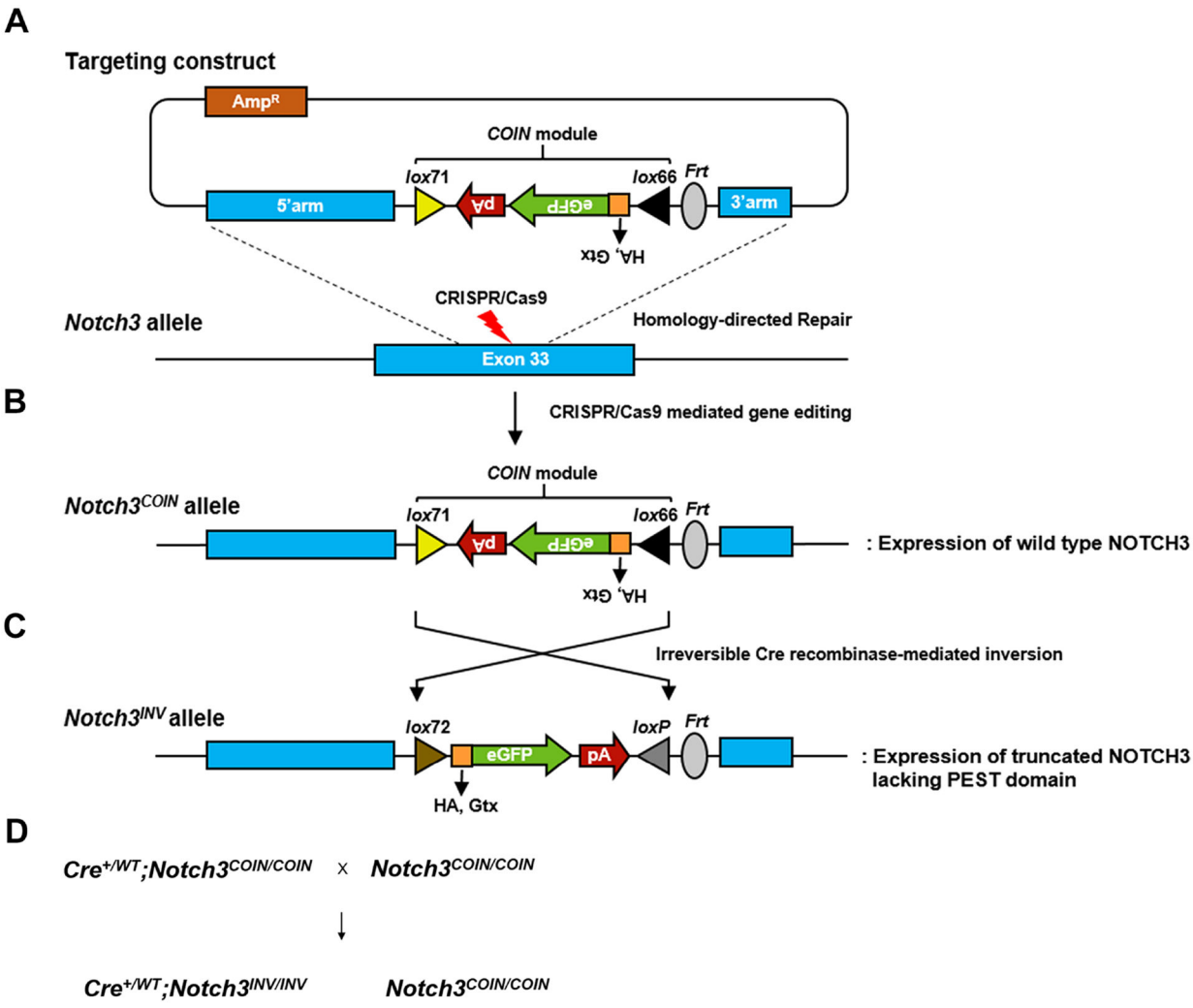

Figure 1. Engineering of the *Notch3*^{COIN} allele.

A. Representation of the targeting construct and silent *COIN* module in the anti-sense orientation consisting of *lox71*, rabbit β-globin (*Rbg*) polyadenylation signal (pA), enhanced green fluorescence protein (eGFP)-coding sequence, Gtx internal ribosome entry site, human influenza hemagglutinin (HA) tag coding sequence, 3'-splice region from the second intron of the *Rbg* gene (not shown) and *lox66*. B. Representation of CRISPR-Cas9 gene editing, and C. Generation of the *Notch3*^{INV} allele by Cre recombinase-mediated inversion of the *COIN* module, and maturation of the *Notch3*^{INV} transcript, which is translated into a NOTCH3 mutant protein lacking the PEST domain. D. Mating scheme

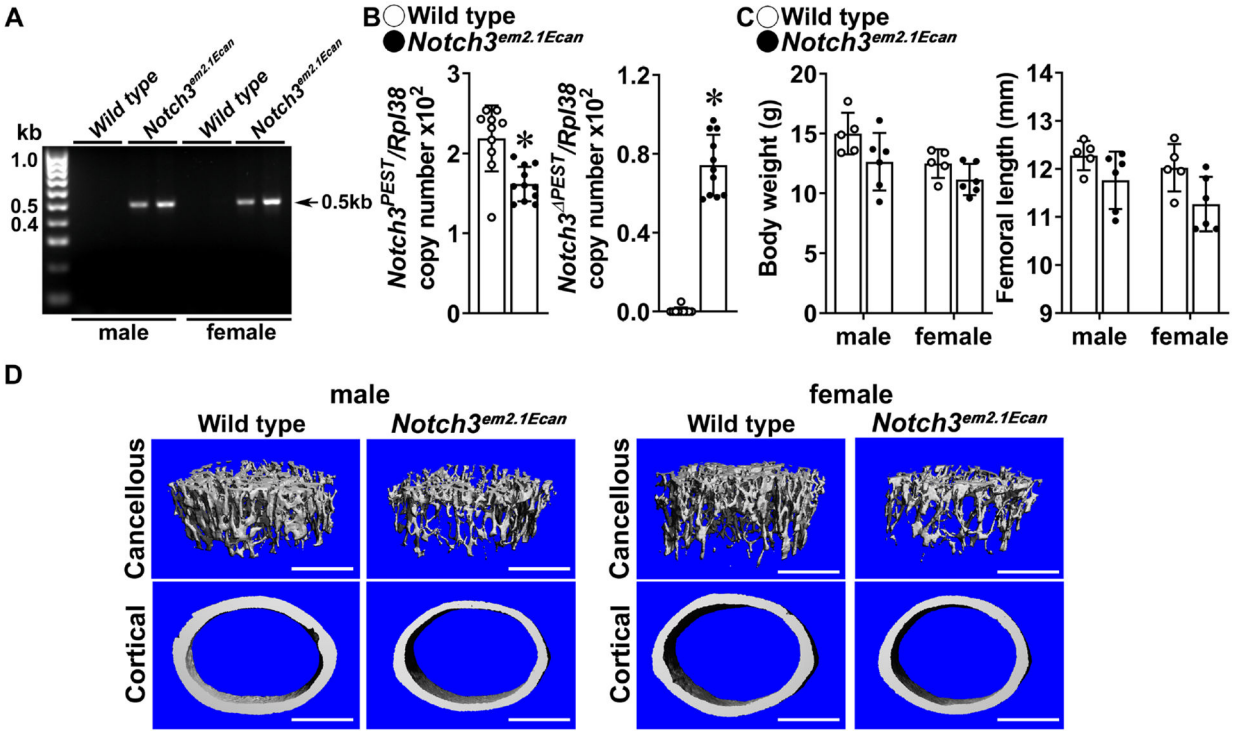

Figure 2. Inversion of the *Notch3*^{COIN} allele in the germ line causes osteopenia.

A. DNA was extracted from tail of heterozygous *Notch3*$^{em2.1Ecan}$ (*Hprt-Cre;Notch3*$^{INV/WT}$) and wild type littermate controls and *Notch3*^{COIN} inversion was documented by gel electrophoresis of PCR products obtained with primers specific for the *Notch3*^{INV} allele. Arrows indicate the position of the 495 base pair (bp) amplicon. B. Total RNA was extracted from calvariae of 1 month old *Notch3*$^{em2.1Ecan}$ mutants (closed circles) and wild type littermate controls (open circles), and expression of the *Notch3* ^{PEST} and *Notch3*$^{\Delta PEST}$ mRNA measured by qRT-PCR. Transcript levels are reported as copy number corrected for *Rpl38* mRNA levels. Bars represent means and ranges S.D.; n = 9 for control, n = 11 for *Notch3*$^{em2.1Ecan}$, all biological replicates. C. Weight in gm and femoral length in mm of 1 month old *Notch3*$^{em2.1Ecan}$ (closed circles) and wild type control littermates (open circles). Bars represent means and ranges SD; n = 5 for control males and females, n = 6 for *Notch3*$^{em2.1Ecan}$ males and females. D. Representative μCT images of femoral proximal trabecular bone and midshaft cortical bone of 1 month old control and *Notch3*$^{em2.1Ecan}$ mice. The scale bar in the right corner represents 500 μm. Complete data set in Table 3. *Significantly different between control and *Notch3*$^{em2.1Ecan}$, $p < 0.05$ by unpaired *t*-test for Panel B and ANOVA for Panel C.

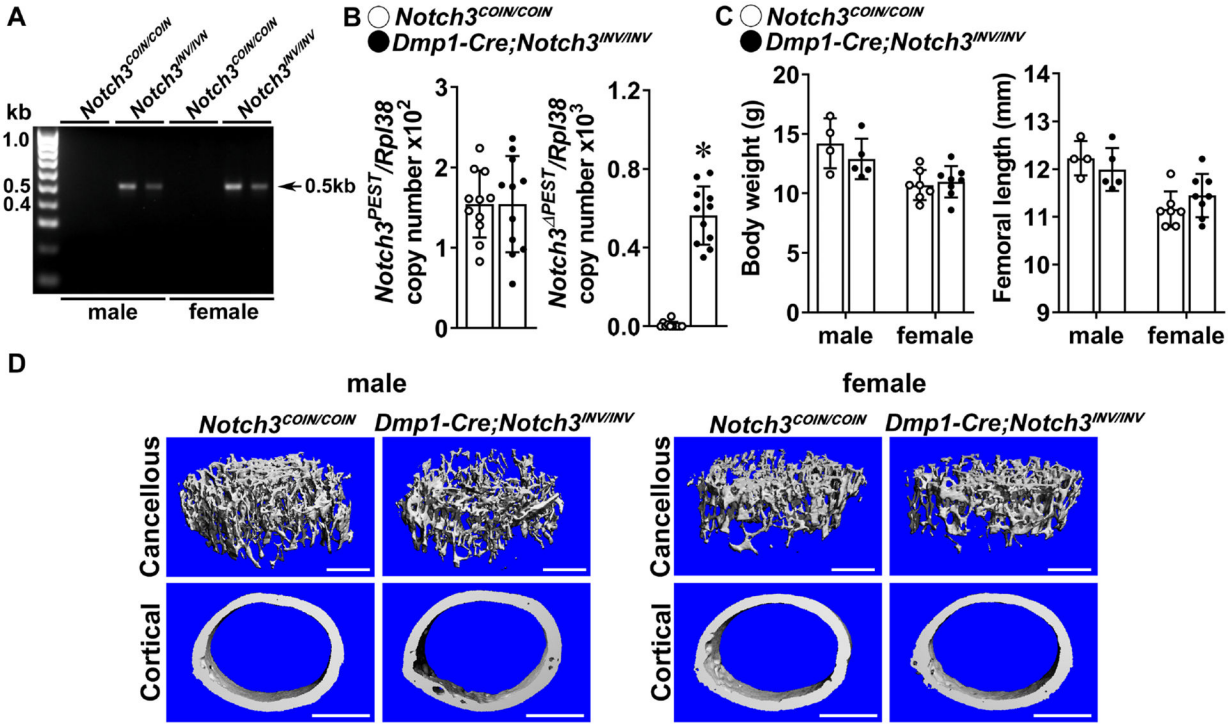

Figure 3. Inversion of the *Notch3*^{COIN} allele in osteocytes causes osteopenia.

A. DNA was extracted from tibiae and *Notch3*^{COIN} inversion was documented by gel electrophoresis of PCR products obtained with primers specific for the *Notch3*^{INV} allele. Arrow indicates the position of the 495 bp amplicon. B. Total RNA was extracted from calvariae, and expression of the *Notch3*^{PEST} and *Notch3*$^{\Delta PEST}$ mRNA measured by qRT-PCR of 1 month old *Dmp1-Cre;Notch3*$^{INV/INV}$ mutants (closed circles) and *Notch3*$^{COIN/COIN}$ littermate controls (open circles). Transcript levels are reported as copy number corrected for *Rpl38* levels. Bars represent means and ranges S.D.; n = 4 for control, n = 4 for *Dmp1-Cre;Notch3*$^{INV/INV}$, all biological replicates. C. Weight in gm and femoral length in mm of 1 month old *Dmp1-Cre;Notch3*$^{INV/INV}$ (closed circles) and *Notch3*$^{COIN/COIN}$ littermate controls (open circles). Bars represent means and ranges SD; n = 4 males and n = 7 females for control, and n = 5 males and n = 8 females for *Notch3*$^{INV/INV}$. D. Representative μCT images of femoral proximal trabecular bone and midshaft cortical bone of 1 month old control *Notch3*$^{COIN/COIN}$ and *Dmp1-Cre;Notch3*$^{INV/INV}$ male and female mice. The scale bar in the right corner represents 500 μm. Complete data set in Table 5. *Significantly different between control *Notch3*$^{COIN/COIN}$ and *Dmp1-Cre;Notch3*$^{INV/INV}$, $p < 0.05$ by unpaired *t*-test.

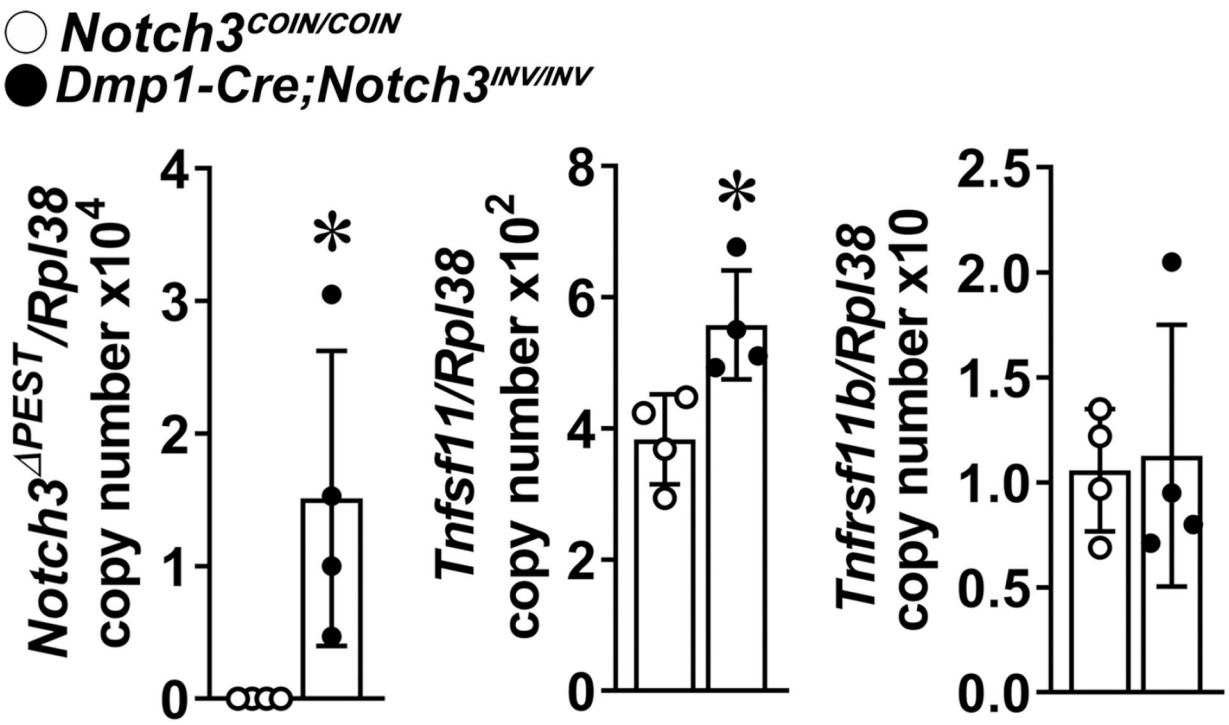

Figure 4. Inversion of the *Notch3*^{COIN} allele in osteocytes induces RANKL.

Total RNA isolated from osteocyte-enriched cells from *Dmp1-Cre;Notch*$^{INV/INV}$ (closed circles) and *Notch3*$^{COIN/COIN}$ control (open circles) mice was extracted, and gene expression was determined by qRT-PCR. Data are expressed as *Notch3*$^{\Delta PEST}$, *Tnfsf11* (RANKL) and *Tnfrsf11b* (osteoprotegerin) copy number corrected for *Rpl38*. Bars represent means and ranges SD; n = 4. Data are derived from biological replicates. *Significantly different between control *Notch3*$^{COIN/COIN}$ and *Dmp1-Cre;Notch3*$^{INV/INV}$, $p < 0.05$ by unpaired *t*-test.

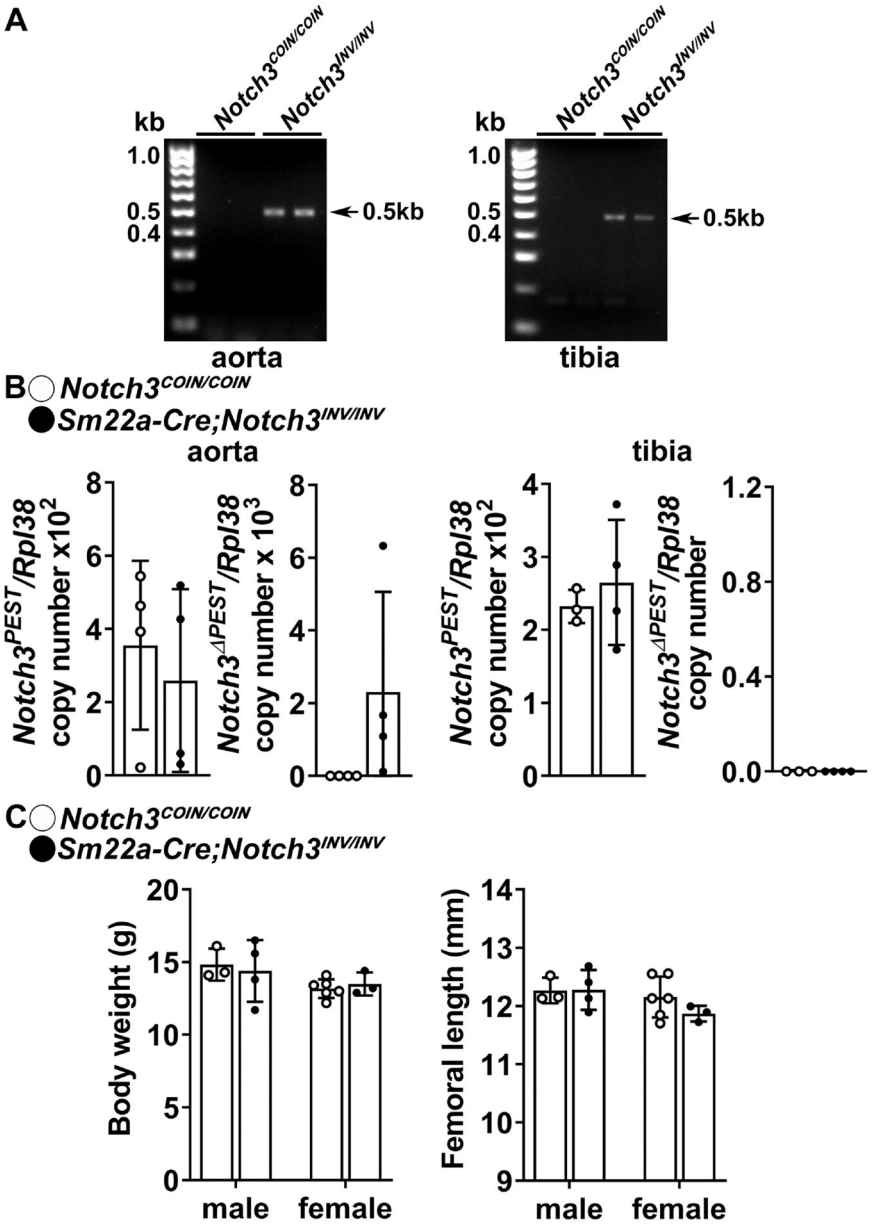

Figure 5. Inversion of the *Notch3*^{COIN} allele in smooth muscle cells does not cause osteopenia.

A. DNA was extracted from aorta and tibiae, and *Notch3*^{COIN} inversion was documented by gel electrophoresis of PCR products obtained with primers specific for the *Notch3*^{INV} allele. Arrows indicate the position of the 495 bp amplicon. B. Total RNA was extracted from aorta and tibiae, and expression of the *Notch3*^{PEST} and *Notch3*$^{\Delta PEST}$ mRNA measured by qRT-PCR in 1 month old *Sm22a-Cre;Notch3*$^{INV/INV}$ mutants (closed circles) and *Notch3*$^{COIN/COIN}$ littermate controls (open circles). Transcript levels are reported as copy number corrected for *Rpl38* levels. Bars represent means and ranges S.D.; n = 3–4 for control and n = 4 for *Sm22a-Cre;Notch3*$^{INV/INV}$, all biological replicates. C. Weight in gm and femoral

length in mm of 1 month old *Sm22a-Cre;Notch3*$^{INV/INV}$ (closed circles) and *Notch3*$^{COIN/COIN}$ littermates (open circles). Bars represent means and ranges SD; n = 3 males and n = 6 females for control and n = 4 males and n = 3 females for *Sm22a-Cre;Notch3*^{INV}.

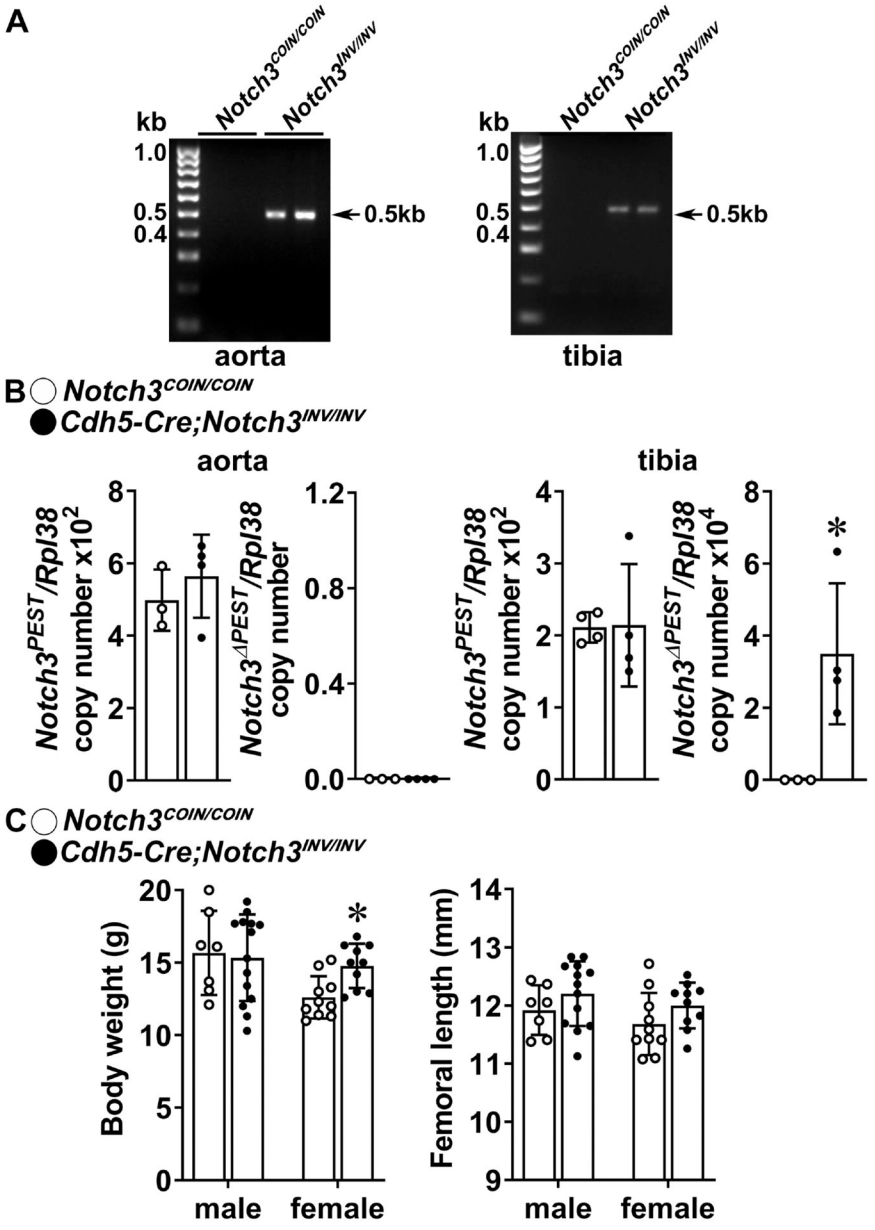

Figure 6. Inversion of the *Notch3*^{COIN} allele in endothelial cells does not cause osteopenia.

A. DNA was extracted from aorta and tibiae and *Notch3*^{COIN} inversion was documented by gel electrophoresis of PCR products obtained with primers specific for the *Notch3*^{INV} allele. Arrows indicate the position of the 495 bp amplicon. B. Total RNA was extracted from aorta and tibiae, and expression of the *Notch3*^{PEST} and *Notch3*$^{\Delta PEST}$ mRNA measured by qRT-PCR in 1 month old *Cdh5-Cre;Notch3*$^{INV/INV}$ mutants (closed circles) and *Notch3*$^{COIN/COIN}$ littermate controls (open circles). Transcript levels are reported as copy number corrected for *Rpl38* mRNA levels. Bars represent means and ranges S.D.; n = 3–4 for control and n = 4 *Cdh5-Cre;Notch3*$^{INV/INV}$, all biological replicates. C. Weight in gm and femoral length in mm of 1 month old *Cdh5-Cre;Notch3*$^{INV/INV}$ (closed circles) and *Notch3*$^{COIN/COIN}$ littermates (open circles). Bars represent means and ranges SD; n = 7 males and n =

10 females for control and n = 14 males and n = 10 females for *Cdh5-Cre;Notch3*$^{INV/INV}$.
*Significantly different between control *Notch3*$^{COIN/COIN}$ and *Cdh5-Cre;Notch3*$^{INV/INV}$, $p < 0.05$ by unpaired *t*-test.

Table 1.

Primers used for allele identification.

Allele	Strand	Sequence	Amplicon Size (bp)
Genotyping			
Cdh5-Cre	Forward	5'-GCGGTCTGGCAGTAAAAACTATC -3'	100
	Reverse	5'-GTGAAACAGCATTGCTGTCACTT-3'	
Dmp1-Cre	Forward	5'-CCCGCAGAACCTGAAGATG-3'	534
	Reverse	5'-GACCCGGCAAAACAGGTAG-3'	
Hprt^{WT}	Forward	5'-TTTCTATAGGACTGAAAGACTTGCTC-3'	200
	Reverse	5'-CACAGTAGCTCTTCAGTCTGATAAAA-3'	
Hprt^{Cre}	Forward	5'-GCGGTCTGGCAGTAAAAACTATC-3'	100
	Reverse	5'-GTGAAACAGCATTGCTGTCACTT-3'	
Notch3	Forward	5'-GAGGCCCAAGGAATCGAGAC-3'	269
	Reverse	5'-ATGAGACGTTTTCTCCGAGTTCAG-3'	
Notch3^{COIN}	Forward	5'-CCGGGCCGCGACTGAAACCCTAG-3'	158
	Reverse	5'-GGTGGGGCTACTGCGGGTTCCTG-3'	
Sm22a-Cre	Forward	5'-GCGGTCTGGCAGTAAAAACTATC -3'	100
	Reverse	5'-GTGAAACAGCATTGCTGTCACTT -3'	
LoxP Recombination			
Notch3^{INV}	Forward	5'- CTGCTCCAGGACATGGAGAGG -3'	Non rec no band
	Reverse	5'- CACGTCGTAGGGGTACTGTAGG -3'	Rec = 495

Table 2.

Primers used for qRT-PCR determinations. GenBank accession numbers identify transcript recognized by primer pairs.

Gene	Strand	Sequence	GenBank Accession Number
Alpl	Forward	5'-TGGTATGGGCGTCTCCACAGTAACC-3'	NM_007431
	Reverse	5'-CTTGGAGAGGGCCACAAAGG-3'	
Bglap	Forward	5'-GACTCCGGCGCTACCTTGGGTAAG-3'	NM_001037939
	Reverse	5'-CCCAGCACAACTCCTCCCTA-3'	
Notch3^{PEST} *	Forward	5'-CATCCTTATTTGACCCCGTC-3'	NM_008716
	Reverse	5'-TGGCATTGGTAGCAGTTG-3'	
Notch3$^{\Delta PEST(HA\ tag)}$**	Forward	5'-AGTTTCTCCCCAAGAGCG-3'	Not applicable
	Reverse	5'-TAGTCGGGCACGTCGTAG-3'	
Rpl38	Forward	5'-AGAACAAGGATAATGTGAAGTTCAAGGTTC-3'	NM_001048057; NM_001048058;
	Reverse	5'-CTGCTTCAGCTTCTCTGCCTTT-3'	NM_023372
Sost	Forward	5'-AGGAATGATGCCACAGAGGTC-3'	NM_024449
	Reverse	5'-CTGGTTGTTCTCAGGAGGAGGCTC-3'	
Tnfrsf11b	Forward	5′-CAGAAAGGAAATGCAACACATGACAAC-3′	NM_008764
	Reverse	5′-GCCTCTTCACACAGGGTGACATC-3′	
Tnfsf11	Forward	5'-TATAGAATCCTGAGACTCCATGAAAAC-3'	NM_011613
	Reverse	5'-CCCTGAAAGGCTTGTTTCATCC-3'	

* recognizes a fragment coding for the PEST domain of NOTCH3 so that it amplifies the product from wild type and non-inverted (floxed) allele, but not from inverted alleles.

** recognizes a fragment coding for the HA tag of the truncated NOTCH3 so that it amplifies only the product from an inverted allele.

Table 3.

Femoral microarchitecture assessed by μCT of 1 month old *Notch3*$^{em2.1Ecan}$ (*Hprt-Cre;Notch3*$^{INV/WT}$) mice and sex-matched wild type littermates (Control).

	Males		Females	
	Control	***Notch3*** ^{INV}	**Control**	***Notch3*** ^{INV}
	n = 5	**n = 6**	**n = 5**	**n = 6**
Distal Femur Trabecular Bone				
Bone Volume/Total Volume (%)	12.5 ± 2.5	6.7 ± 1.8 *	9.0 ± 1.2	5.0 ± 0.7 *
Trabecular Separation (μm)	195 ± 10	251 ± 30 *	216 ± 14	288 ± 16 *
Trabecular Number (1/mm)	5.3 ± 0.2	4.1 ± 0.5 *	4.7 ± 0.3	3.5 ± 0.2 *
Trabecular Thickness (μm)	35 ± 3	31 ± 3 *	31 ± 1	29 ± 1
Connectivity Density (1/mm^3)	411 ± 77	223 ± 54 *	299 ± 60	169 ± 29 *
Structure Model Index	1.9 ± 0.3	2.5 ± 0.1 *	2.2 ± 1.1	2.5 ± 0.1 *
Density of Material (mg HA/cm^3)	775 ± 8	753 ± 12 *	776 ± 7	764 ± 8
Femoral Midshaft Cortical Bone				
Bone Volume/Total Volume (%)	82.0 ± 1.4	80.3 ± 2.5	82.4 ± 0.7	81.2 ± 0.9
Porosity (%)	18.0 ± 1.4	19.7 ± 2.5	17.6 ± 0.7	18.8 ± 0.9
Cortical Thickness (μm)	88 ± 5	82 ± 9	86 ± 2	80 ± 4
Total Area (mm^2)	1.5 ± 0.1	1.4 ± 0.1	1.5 ± 0.1	1.4 ± 0.1
Bone Area (mm^2)	0.49 ± 0.03	0.42 ± 0.05 *	0.45 ± 0.02	0.41 ± 0.03
Marrow Area (mm^2)	1.0 ± 0.1	1.0 ± 0.1	1.0 ± 0.1	1.0 ± 0.1
Periosteal Perimeter (μm)	4.4 ± 0.1	4.2 ± 0.2	4.3 ± 0.1	4.1 ± 0.2
Endocortical Perimeter (mm)	3.6 ± 0.3	3.5 ± 0.2	3.6 ± 0.1	3.5 ± 0.2
Density of Material (mg HA/cm^3)	960 ± 20	946 ± 23	974 ± 10	962 ± 11

μCT was performed at the femoral distal end for trabecular or midshaft for cortical bone. Values are means ± S.D.

*Significantly different between control and *Notch3*$^{em2.1Ecan}$ mice, $p < 0.05$ by ANOVA.

Table 4.

Cancellous bone histomorphometry of 1 month old *Notch3*$^{em2.1Ecan}$ (*Hprt-Cre;Notch3*$^{INV/WT}$) male mice and sex-matched wild type littermates (controls).

	Males	
Cancellous Bone	**Control n = 5**	***Notch3*^{INV} n = 4**
Static Histomorphometry		
Bone Volume/Tissue Volume (%)	16.3 ± 2.8	9.6 ± 5.0 *
Trabecular Separation (μm)	195 ± 26	355 ± 152 *
Trabecular Number (1/mm)	4.3 ± 0.4	2.8 ± 0.9 *
Trabecular Thickness (μm)	38 ± 5	32 ± 1
Osteoblast Surface/Bone Surface (%)	21.2 ± 4.8	21.6 ± 8.6
Osteoblasts/Bone Perimeter (1/mm)	16.8 ± 4.6	17.4 ± 6.3
Osteoid Surface/Bone Surface (%)	1.7 ± 0.9	1.2 ± 0.9
Osteoclast Surface/Bone Surface (%)	9.7 ± 2.5	9.8 ± 4.7
Osteoclasts/Bone Perimeter (1/mm)	3.6 ± 0.9	3.6 ± 1.8
Eroded Surface/Bone Surface (%)	2.3 ± 0.8	2.0 ± 1.5

Histomorphometry was carried out on sagittal sections of distal femurs. Values are means ± S.D.

* Significantly different between control and *Notch3*$^{em2.1Ecan}$ mice, $p < 0.05$ by unpaired *t*-test.

Table 5.

Femoral microarchitecture assessed by μCT of 1 month old *Dmp1-Cre;Notch3*$^{INV/INV}$ mice and sex-matched *Notch3*^{em2Ecan} (*Notch3*$^{COIN/COIN}$) littermate controls.

	Males		**Females**	
	Notch3 ^{COIN}	***Notch3*** ^{INV}	***Notch3*** ^{COIN}	***Notch3*** ^{INV}
	n = 4	**n = 5**	**n = 7**	**n = 8**
Distal Femur Trabecular Bone				
Bone Volume/Total Volume (%)	10.0 ± 1.2	7.6 ± 1.3 *	6.2 ± 1.3	5.8 ± 1.3
Trabecular Separation (μm)	200 ± 10	222 ± 19	268 ± 33	279 ± 24
Trabecular Number (1/mm)	5.0 ± 0.3	4.6 ± 0.4	3.8 ± 0.5	3.7 ± 0.3
Trabecular Thickness (μm)	31 ± 0	30 ± 1	30 ± 1	29 ± 2
Connectivity Density (1/mm^3)	329 ± 52	230 ± 55	197 ± 70	195 ± 42
Structure Model Index	2.1 ± 0.2	2.4 ± 0.2	2.4 ± 0.2	2.3 ± 0.3
Density of Material (mg HA/cm^3)	767 ± 17	761 ± 10	751 ± 12	741 ± 20
Femoral Midshaft Cortical Bone				
Bone Volume/Total Volume (%)	83.4 ± 1.4	82.7 ± 1.3	81.1 ± 1.2	80.2 ± 2.4
Porosity (%)	16.6 ± 1.4	17.3 ± 1.3	18.9 ± 1.2	19.8 ± 2.4
Cortical Thickness (μm)	91 ± 6	87 ± 5	81 ± 4	80 ± 6
Total Area (mm^2)	1.5 ± 0.2	1.4 ± 0.1	1.4 ± 0.1	1.4 ± 0.2
Bone Area (mm^2)	0.47 ± 0.04	0.44 ± 0.05	0.41 ± 0.03	0.41 ± 0.05
Marrow Area (mm^2)	1.0 ± 0.1	1.0 ± 0.1	0.9 ± 0.1	1.0 ± 0.2
Periosteal Perimeter (μm)	4.3 ± 0.2	4.2 ± 0.2	4.1 ± 0.2	4.2 ± 0.3
Endocortical Perimeter (mm)	3.6 ± 0.2	3.5 ± 0.1	3.5 ± 0.1	3.5 ± 0.3
Density of Material (mg HA/cm^3)	959 ± 27	956 ± 27	929 ± 15	917 ± 3

μCT was performed at the femoral distal end for trabecular or midshaft for cortical bone. Values are means ± S.D.

* Significantly different between control and *Notch3*$^{INV/INV}$ mice, $p < 0.05$ by unpaired ANOVA.

Table 6.

Femoral microarchitecture assessed by μCT of 1 month old *Sm22a-Cre;Notch3*$^{INV/INV}$ mice and *Notch3*^{em2Ecan} (*Notch3*$^{COIN/COIN}$) sex-matched littermate controls.

	Males		Females	
	Notch3 ^{COIN}	***Notch3*** ^{INV}	***Notch3*** ^{COIN}	***Notch3*** ^{INV}
	n = 3	**n = 4**	**n = 6**	**n = 3**
Distal Femur Trabecular Bone				
Bone Volume/Total Volume (%)	6.9 ± 1.1	5.9 ± 1.7	4.7 ± 0.8	4.5 ± 0.4
Trabecular Separation (μm)	252 ± 31	274 ± 28	320 ± 32	316 ± 36
Trabecular Number (1/mm)	4.0 ± 0.4	3.7 ± 0.2	3.2 ± 0.3	3.3 ± 0.3
Trabecular Thickness (μm)	33 ± 2	33 ± 2	33 ± 2	32 ± 1
Connectivity Density (1/mm^3)	155 ± 44	117 ± 33	95 ± 21	94 ± 33
Structure Model Index	2.4 ± 0.1	2.6 ± 0.2	2.6 ± 0.1	2.6 ± 0.1
Density of Material (mg HA/cm^3)	784 ± 7	778 ± 13	762 ± 15	774 ± 4
Femoral Midshaft Cortical Bone				
Bone Volume/Total Volume (%)	82.6 ± 1.5	83.2 ± 1.1	82.3 ± 1.5	82.9 ± 1.2
Porosity (%)	17.5 ± 1.5	16.8 ± 1.1	17.7 ± 1.5	17.1 ± 1.2
Cortical Thickness (μm)	89 ± 2	95 ± 4	90 ± 15	93 ± 6
Total Area (mm^2)	1.6 ± 0.1	1.5 ± 0.1	1.6 ± 0.1	1.6 ± 0.1
Bone Area (mm^2)	0.50 ± 0.03	0.50 ± 0.04	0.50 ± 0.01	0.51 ± 0.02
Marrow Area (mm^2)	1.1 ± 0.1	1.0 ± 0.1	1.1 ± 0.1	1.1 ± 0.1
Periosteal Perimeter (μm)	4.4 ± 0.1	4.3 ± 0.2	4.4 ± 0.1	4.5 ± 0.1
Endocortical Perimeter (mm)	3.7 ± 0.1	3.5 ± 0.2	3.6 ± 0.1	3.7 ± 0.1
Density of Material (mg HA/cm^3)	964 ± 20	972 ± 18	960 ± 21	969 ± 9

μCT was performed at the femoral distal end for trabecular or midshaft for cortical bone. Values are means ± S.D.

Table 7.

Femoral microarchitecture assessed by μCT of 1 month old *Cdh5-Cre;Notch3*$^{INV/INV}$ mice and *Notch3*^{em2Ecan} (*Notch3*$^{COIN/COIN}$) sex-matched littermate controls.

	Males		Females	
	Notch3 ^{COIN}	***Notch3*** ^{INV}	***Notch3*** ^{COIN}	***Notch3*** ^{INV}
	n = 7	**n = 14**	**n = 10**	**n = 10**
Distal Femur Trabecular Bone				
Bone Volume/Total Volume (%)	7.5 ± 1.7	8.1 ± 1.7	5.1 ± 0.1	5.7 ± 0.8
Trabecular Separation (μm)	250 ± 20	241 ± 18	289 ± 31	284 ± 33
Trabecular Number (1/mm)	4.1 ± 0.3	4.2 ± 0.3	3.5 ± 0.4	3.6 ± 0.4
Trabecular Thickness (μm)	34 ± 5	35 ± 4	30 ± 2	32 ± 1
Connectivity Density (1/mm^3)	176 ± 28	199 ± 42	140 ± 53	136 ± 31
Structure Model Index	2.4 ± 0.2	2.3 ± 0.2	2.5 ± 0.1	2.4 ± 0.1
Density of Material (mg HA/cm^3)	765 ± 23	778 ± 18	763 ± 16	766 ± 14
Femoral Midshaft Cortical Bone				
Bone Volume/Total Volume (%)	81.4 ± 2.3	82.3 ± 2.0	82.0 ± 1.4	82.8 ± 1.3
Porosity (%)	18.6 ± 2.3	17.7 ± 2.0	18.0 ± 1.4	17.2 ± 1.3
Cortical Thickness (μm)	89 ± 8	91 ± 10	87 ± 5	91 ± 5
Total Area (mm^2)	1.5 ± 0.2	1.5 ± 0.2	1.4 ± 0.1	1.5 ± 0.1
Bone Area (mm^2)	0.50 ± 0.07	0.51 ± 0.08	0.44 ± 0.03	0.49 ± 0.03
Marrow Area (mm^2)	1.0 ± 0.1	1.0 ± 0.1	0.9 ± 0.1	1.0 ± 0.1
Periosteal Perimeter (μm)	4.3 ± 0.2	4.4 ± 0.2	4.2 ± 0.1	4.3 ± 0.2
Endocortical Perimeter (mm)	4.3 ± 0.2	3.6 ± 0.2	3.4 ± 0.1	3.6 ± 0.2
Density of Material (mg HA/cm^3)	949 ± 34	961 ± 22	957 ± 23	965 ± 18

μCT was performed at the femoral distal end for trabecular or midshaft for cortical bone. Values are means ± S.D.

*Significantly different between control and *Notch3*$^{INV/INV}$ mice by unpaired ANOVA.